The 8th European Congress on Computational Methods in Applied Sciences and Engineering
ECCOMAS Congress 2022
5-–9 June 2022, Oslo, Norway

PHASE FIELD MODEL FOR SIMULATING FRACTURE OF ICE

Rabea E. Sondershaus[1*], Ralf Müller[2]

[1] Fachgebiet Kontinuumsmechanik, Technische Universität Darmstadt,
Franziska-Braun-Straße 7, 64287 Darmstadt, Germany
rabea.sondershaus@tu-darmstadt.de

[2] Fachgebiet Kontinuumsmechanik, Technische Universität Darmstadt,
Franziska-Braun-Straße 7, 64287 Darmstadt, Germany
ralf.mueller@mechanik.tu-darmstadt.de

Key words: phase field model, fracture, ice, application

Abstract.

In the last decade, the phase field model has been established to simulate crack nucleation as well as crack propagation. In this variational approach the physically discontinuity of a crack is modeled by a continuous field variable that distinguishes between intact and broken material. The phase field model has been recently extended to viscoelastic materials in various ways, in which the rate dependent response of viscoelastic materials are taken into account.

We propose a viscoelastic fracture phase field model and apply it to simulate the fracture in ice shelves. Thereby we consider the viscoelastic rheology of ice, which can be represented by a Maxwell model. The elastic response is often neglected in ice dynamic simulations but crucial for fracture mechanical studies.

The numerical examples of this contribution are implemented and conducted in the finite element software FEniCS and data mimic typical situations in Antarctic and Greenland ice shelves.

1 INTRODUCTION

Based in Griffith concept of energy release rates Margio and Francfort [1] presented a variational formulation of fracture mechanics which was transformed into the phase field method for fracture by Bourdin [2, 3, 4]. Since then, the phase field method is widely used to simulate fracture processes, due to its simple and robust numerical implementation. Another advantage of this method is its ability to simulate crack initiation as well as crack propagation and also crack branching. In the last decade the approach has been modified in various ways to study for example the influence of the degradation function [5, 6, 7] or the driving force by using different splitting schemes [8, 9, 10, 11].

The method has been extended from brittle to dynamic fracture [12, 13, 14, 15, 16] and fatigue failure [17, 18, 19, 20, 21]. Furthermore, various material behaviors such as anisotropy [22, 23, 24, 25, 26], plasticity [27, 28, 29, 30, 31] and also viscoelasticity [32, 33, 34, 35] were studied. In the viscoelastic case, attention was only given to solid like behavior.

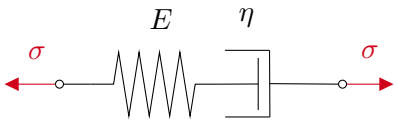

Figure 1: The Maxwell material can be used to represent the rheology of ice [43]. It consists of an elastic spring characterized by Young's modulus E and a damper with a viscosity η. The series connection of the elements results in an elastic response of the material on short time scales and a viscous response on long time scales [42].

In this paper we apply the phase field method for fracture to the research field of glaciers and simulate fractures in ice shelves. Ice shelves are the floating extensions of glaciers, which flow due to the gravity into the ocean. The ice shelf is still connected to its corresponding glacier and fed by it. At the terminus of the ice shelf to the ocean, called the calving front, cracks form and ice breaks away, resulting in ice bergs. The calving of icebergs is one of the predominating mass loss mechanisms in Greenland. The mass loss can be enhanced due to major break up events of ice shelves. This is because the floating parts of outlet glaciers play an important role regarding the stability of the inland ice by buttressing it. If the ice shelf disintegrates the respective glacier speeds up and has therefore a higher contribution to sea level rise. Examples for such disintegration events can be found at Zachariæice stream [36] and Jakobshavn Isbræ [37] in Greenland or the Wilkins ice shelf [38] in Antarctica. It is therefore important to investigate the formation of cracks within an ice shelf in order to better understand the dynamics at the calving front.

As cracks do not always travel through the entire ice shelf immediately, but can also remain stable for a longer period of time due to the complex stress situation, it is significant to consider the viscoelastic rheology of ice. Ice acts like an elastic material on short time scales but on long time scales it can be described as a viscous fluid. Therefore ice is a viscoelastic fluid.

Existing models describing the long term behavior of glaciers and ice sheets, often neglect the elastic response of the material, including only viscous flow. However, recent studies have shown that measured deformations can only be explained by considering the viscoelastic material behavior of ice [39, 40, 41]. Another drawback of existing ice sheet models is the way the process of calving is described. Often simple assumptions of calving rates or stress based criteria are used. Both cases are strong simplifications of the calving process. To overcome these simplifications, we propose a viscoelastic phase field model to simulate fracture in ice shelves and apply our model to a typical situation leading to calving, which can be found in Greenland as well as in Antarctica.

2 MODEL

In this section the constitutive model for ice is presented. Subsequently the phase field method for fracture is introduced.

2.1 Ice rheology

Ice shows a viscoelastic material behavior. Phenomena like the calving of ice bergs illustrate its short term elastic material response. On the other hand the flow of glaciers shows the viscous

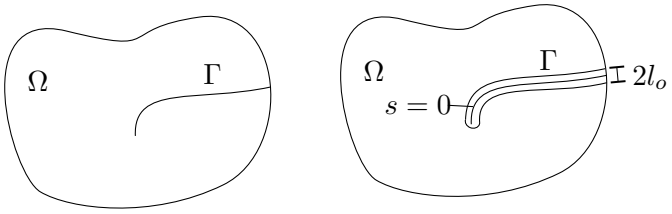

Figure 2: In the left panel a domain Ω with a sharp crack interface Γ is shown. On the right side the crack is approximated by the continuous scalar field s which varies between intact $s = 1$ and fully broken $s = 0$ material within the crack width l_0.

behavior on longer time scales. A material of this kind can be represented by a Maxwell model shown in Figure 1 [43]. The Maxwell material model consists of two rheological elements. An elastic and a viscous one, connected in series and characterized by Young's modulus E and the shear viscosity η, respectively. Due to the series connection it can be assumed that the stress acting on the elastic element σ^e and the stress acting on the viscous element σ^v are equal to the stress applied to the material model σ:

$$\sigma = \sigma^e = E\varepsilon^e = \sigma^v = \eta\dot{\varepsilon}^v \quad . \tag{1}$$

Hence the constitutive relations of the elastic element and the viscous element can be equalized. The overall strain of the Maxwell model ε is the sum of the elastic strain ε^e and the viscous strain ε^v:

$$\varepsilon = \varepsilon^e + \varepsilon^v \quad . \tag{2}$$

Combining Equations (1) and (2) leads to Equations (3) and (4)

$$\sigma = E(\varepsilon - \varepsilon^v) \quad , \tag{3}$$

$$\dot{\varepsilon}^v = \frac{E}{\eta}(\varepsilon - \varepsilon^v) \quad . \tag{4}$$

Where Equation (3) is the constitutive relation for the Maxwell material model in dependency of the viscous strain ε^v which serves as an internal variable. The evolution of this internal variable with respect to time $\dot{\varepsilon}^v$ is described by Equation (4).

2.2 Phase field model for fracture

In the phase field approach for fracture the sharp crack interface is smoothed out and described by an continuous scalar field s. The additional field variable s distinguishes between intact $s = 1$ and fully broken material, where $s = 0$. The concept of an approximated crack compared to a sharp crack can be seen in Figure 2.

Following previous work [33, 35], the pseudo energy potential for a viscoelastic material consists of three parts

$$\Pi \;=\; \int_\Omega \psi^e dV + \int_\Omega \psi^f dV + \int_\Omega \psi^v dV \tag{5}$$

the elastic strain energy, the fracture energy and the viscous energy, respectively. The elastic strain energy density can be decomposed into its volumetric ψ^e_{vol} and deviatoric part ψ^e_{dev}

$$\begin{aligned} \psi^e = & \quad \psi^e_{vol} & +\psi^e_{dev} \\ = & \quad \tfrac{1}{2}K\varepsilon^e_{vol} : \varepsilon^e_{vol} & +\mu\varepsilon^e_{dev} : \varepsilon^e_{dev} \quad , \end{aligned}$$

where K is the bulk modulus, μ the shear modulus and ε^e the strain tensor. In infinitesimal strain theory the strain tensor ε^e is given with the displacement u as

$$\varepsilon^e = \frac{1}{2}\left(\nabla u + \nabla u^T\right) \quad .$$

Macaulay brackets

$$\langle x\rangle_+ = \begin{cases} x & x \geq 0 \\ 0 & x < 0 \end{cases} \qquad \langle x\rangle_- = \begin{cases} x & x \leq 0 \\ 0 & x > 0 \end{cases}$$

are used to split the volumetric strain energy into its positive and negative part. By not degrading the negative volumetric part, crack propagation does not take place under compression but only under tensile or shear loading. The elastic energy part ψ^e of the pseudo energy potential Π results in

$$\psi^e = \int_\Omega g(s)\left(\frac{1}{2}K\langle\varepsilon^e_{vol} : \varepsilon^e_{vol}\rangle_+ + \mu\varepsilon^e_{dev} : \varepsilon^e_{dev}\right) + \frac{1}{2}K\langle\varepsilon^e_{vol} : \varepsilon^e_{vol}\rangle_- dV \quad . \tag{6}$$

A widely used quadratic degradation function $g(s) = s^2 + \eta_{RS}$ is used, where $\eta_{RS} \ll 1$ is a small residual stiffness, which is introduced to ensure a numerically well conditioned system for the totally broken phase.

Following the approach by Ambrosio and Tortorelli [44], the energy required to generate new crack surfaces is derived from the following energy density

$$\psi^f = \mathcal{G}_c\left(\frac{s^2}{4l_o} + l_o\nabla s \cdot \nabla s\right) \quad . \tag{7}$$

Here $\mathcal{G}_c$ is the critical energy release rate, a material property connected to the fracture toughness by $K_I = \sqrt{E\mathcal{G}_c}$ for a plane stress state. The parameter l_0 represents the crack width and, in order to provide mesh independent results, should contain at least three mesh elements.

The contribution of the stored viscous energy ψ^v to the total energy is given by

$$\psi^v = \int_\Omega \int_t \frac{1}{2}\eta\dot{\varepsilon}^v : \dot{\varepsilon}^v dV \quad . \tag{8}$$

Compared to Dammaß et al. [35] the viscous energy is not degraded and it is therefore assumed, that no viscous energy acts as a driving force on the crack.

Combining Equations (6), (7) and (8) the pseudo energy potential Π (see Equation (5)) results in

$$\begin{aligned} \Pi = & \int_\Omega g(s)\left(\frac{1}{2}K\langle\varepsilon^e_{vol} : \varepsilon^e_{vol}\rangle_+ + \mu\varepsilon^e_{dev} : \varepsilon^e_{dev}\right) + \frac{1}{2}K\langle\varepsilon^e_{vol} : \varepsilon^e_{vol}\rangle_- dV \\ & + \int_\Omega \mathcal{G}_c\left(\frac{s^2}{4l_o} + l_o\nabla s \cdot \nabla s\right) dV + \int_\Omega \int_t \frac{1}{2}\eta\dot{\varepsilon}^v : \dot{\varepsilon}^v dV \quad . \end{aligned}$$

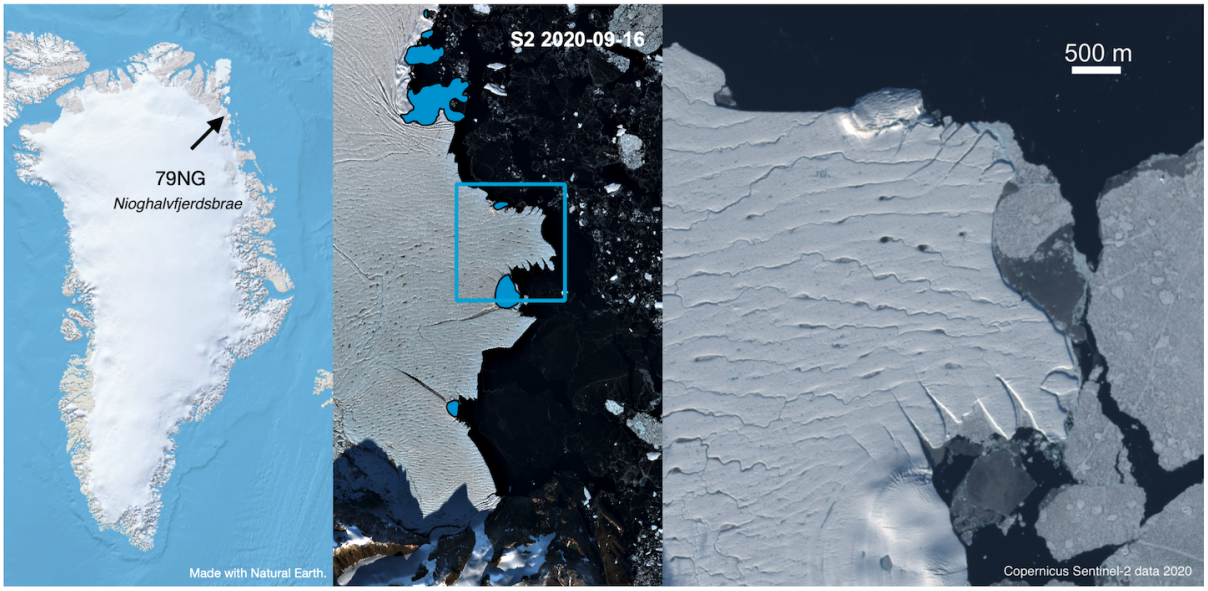

Figure 3: Satellite image of the area of interest. The left panel shows a map of Greenland in which the location of the 79°N glacier is marked. The middle panel shows a satellite image of the floating glacier tongue and its front taken in September of 2020. The glacier is flowing from west to east into the ocean, appearing black in the image. Areas of light blue color show so called pinning points where the ice shelf is grounded. The blue frame indicates the location of the detail shown in the right panel (Copernicus Sentinel-2 data 2020).

The governing equations are derived by means of calculus of variations. By calculating the variation of Π with respect to u the equilibrium in conjunction with the constitutive equation (3) are obtained. The evolution of the phase field parameter s is given by $\dot{s} = -M\delta_s\Pi$. Here the mobility parameter M is enhancing the numerical stability of the system. Furthermore, the variation with respect to ε^v of the time discretised pseudo energy potential $\delta_{\varepsilon^v}\Pi_{\Delta t} = 0$ results in the evolution Equation (4) for the internal variable $\dot{\varepsilon}^v$.

3 NUMERICAL EXAMPLE

The presented model is applied to a typical situation in ice shelves where cracks occur. First, the modelling domain and the associated boundary conditions are described. This is followed by some aspects of the numerical implementation. Afterwards the results of a numerical experiment are presented.

3.1 Modeling domain

To mimic a typical situation found in ice shelves in Greenland and Antarctica, the Nioghalvfjerdsbræ in Greenland is used as a reference domain. The Nioghalvfjerdsbræ, also referred to as 79°N glacier, is one of the largest outlet glaciers of the Greenland ice sheet. Its location and a satellite image of its calving front is shown in Figure 3. At various points the usually floating glacier tongue is grounded, due to mountains. In the middle panel of Figure 3 these so called

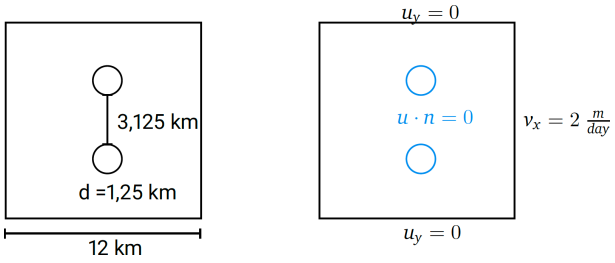

Figure 4: The left panel of the figure shows the two dimensional model domain. It consists of a square plate with an edge length of 12 km. Within this plate two circles with a diameter of 1.25 km each represent idealised pining points. The distance between the pinning points is 3.125 km. In the right panel the boundary conditions used throughout the simulation are indicated. Displacement boundary conditions are described on the outer domain boundary, whereas a no penetration condition is applied to the circle boundary.

pinning points are shown in blue color. On one hand these pinning points provide additional stability to the glacier by buttressing it. On the other hand these features are the onset of cracks as can be clearly seen in the middle and the right panel of the figure. Such pinning points can be found at several ice shelves in Greenland and Antarctica, which is why we want to investigate the formation of cracks at those points.

In a first attempt, a two dimensional model domain including two circular obstacles representing idealised pinning points was created. A similar scenario can be found in the right panel of Figure 3 showing a detailed view of the satellite image. Restricted by two pinning points and with a velocity of approximately $v_x = 2\,\mathrm{m\,day}^{-1}$ the glacier flows from west to east. The corresponding model domain is shown in the left panel of Figure 4. The dimensions of the domain correspond approximately to those of the 79°N glacier in the right panel of Figure 3.

3.2 Boundary conditions

After selecting the model domain, appropriate boundary conditions are needed. We assume that the domain is connected to the rest of the ice shelf and therefore the vertical displacement u_y at the upper and lower boundary is 0. At the right side of the domain a constant velocity of $v_x = 2\,\mathrm{m\,day}^{-1}$ is applied, which is in good agreement with measured velocities of the 79°N glacier. This choice of displacement boundary condition leads to a tension stress state. As the pinning points are fixed, the ice must flow around them. To achieve this a penalty term is added to the pseudo potential Π

$$\Pi + p \int_{\Gamma_{\mathrm{pp}}} \frac{1}{2}(u \cdot n)^2 \, dA = 0 \tag{9}$$

where n is the outer normal vector of the circle boundaries Γ_{pp}. This additional term in the formulation ensures that no ice can flow into the circles, representing the pinning points. A penalty parameter $p = 10 \cdot 10^{10}$ is chosen, which leads to a sufficient compliance of the boundary condition. An overview of these boundary conditions can be found in the right panel of Figure 4.

To ensure irreversibility of fracture, a Dirichlet boundary condition for the phase field variable s is applied in each time step [49, 50].

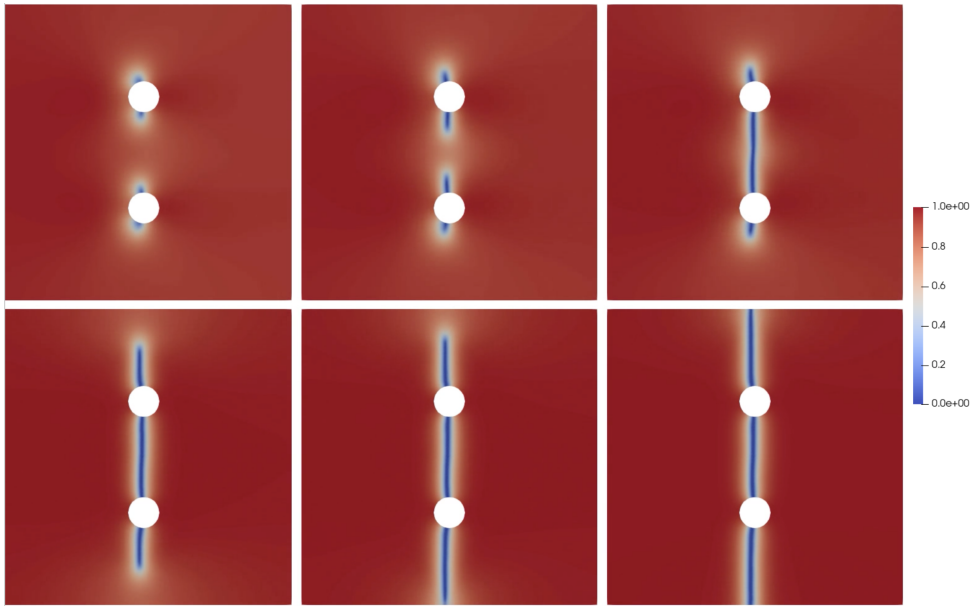

Figure 5: evolution of the phase field s

3.3 Further implementation aspects

The mesh was created using *Gmsh* [46] and the model was implemented in the finite element framework *FEniCS* [47, 48]. An adaptive time stepping algorithm is used, whereby the viscous strain rate $\dot{\varepsilon}^v$ is approximated by a backwards Euler scheme

$$\dot{\varepsilon}^v = \frac{\varepsilon^v_{n+1} - \varepsilon^v_n}{\Delta t} \quad . \tag{10}$$

The material parameters for ice are taken from [43, 45] and can be found in Table 1.

Table 1: Typical material parameters for ice, used throughout the simulation [43, 45].

E	$9 \cdot 10^9$	Pa	Young's modulus
ν	0.325		Poisson's ratio
η	$9 \cdot 10^{14}$	Pa s	viscosity
K_I	$95 \cdot 10^3$	Pa $\mathrm{m}^{1/2}$	fracture toughness

3.4 Results

Figure 5 shows the evolution of the phase field s. At the beginning of the simulation four crack tips form. At each pinning point two crack tips occur, one at the top and one at the bottom. The cracks propagate in vertical direction, perpendicular to the flow direction. First the cracks grow simultaneously at both sides of the pinning points. Then the cracks in the areas between the circle and the outer domain boundary stop growing and only the cracks in the area between the pinning points continue to develop. Figure 6 illustrates this situation. In Figure 6a

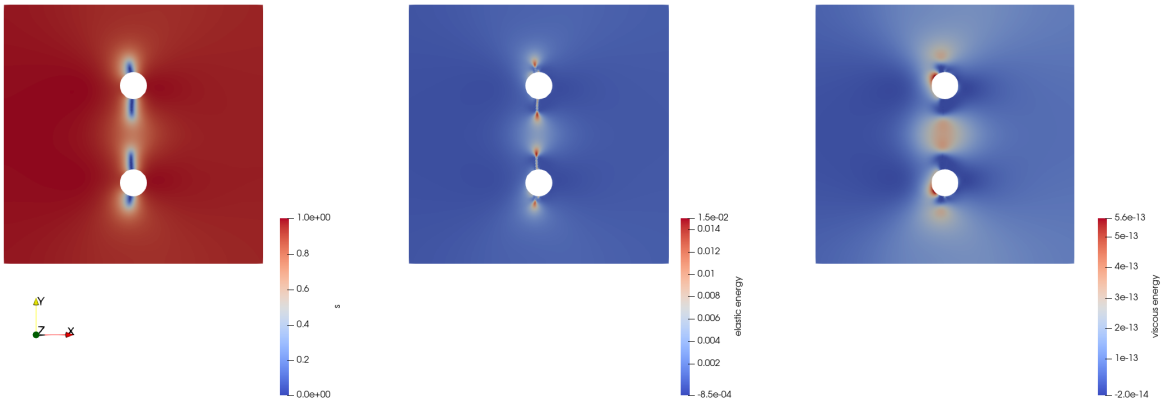

(a) phase field variable s (b) elastic energy ψ^e (c) viscous energy ψ^v

Figure 6: results for the phase field parameter s, the elastic energy ψ^e, and viscous energy ψ^v (plotted using Paraview [51])

the phase field parameter s is shown. Figure 6b and Figure 6c show the corresponding elastic energy ψ^e and viscous energy ψ^v, respectively. The elastic energy is high at the crack tips. It is higher at the tips between the circles than on the other two crack tips. Thus the cracks in the region between the pinning points will continue to develop. In contrast, the viscous energy reaches its maximum in front of the circles, where the ice has to flow around the pinning points. The viscous energy is several orders of magnitudes smaller than the elastic energy. After the crack tips converge between the circles, the crack above the upper ice rise and the crack below the lower ice rise start to grow again until the domain is completely torn. The lower crack reaches the boundary of the domain earlier than the upper crack. The simulation was stopped, once the domain was fully separated.

4 DISCUSSION

The numerical results derived with the phase field method are in good agreement with the observed crack path from the satellite image shown in Figure 3. In both cases a vertical crack path occurs at the ice rises. In comparison to the satellite image of the 79°N glacier the crack tips at the pinning points in our numerical model converge, whereas in the satellite image the cracks stop to evolve and move further in the direction of flow. In addition, new cracks arise at the pinning points. The chosen modeling setup is a first approximation of pinning points in ice shelves. It does not cover the large complexity of real ice shelves yet.

Although the model setup is symmetric, the cracks did not developed symmetrically. The crack below the lower pinning point reaches the domain boundary earlier than the crack above the upper one. The small derivations in the crack evolution probably originate from the triangle mesh used, which is not fully symmetric. Regarding the non symmetric behaviour of the crack path, further investigations need to be carried out to examine influence of the mesh.

According to experiments [52] polycrystalline ice shows a strain rate dependent material behavior, also known as Glen's flow law. To adapt the constitutive model even further to the real behavior of ice, we want to consider this power law in the future.

In this work we only presented simulations in 2D. However the model can be easily extended to a three-dimensional domain, which is subject of current research.

5 CONCLUSIONS

We proposed a viscoelastic phase field model to simulate fracture in ice shelves, which considers a constitutive relation of a Maxwell material. Despite the simplifications of the proposed model in terms of the constitutive equation and the model domain, a good agreement between the cracks in the satellite image and the modeled crack path can be observed. It seems promising that the viscoelastic phase field model can be used in future to simulate fracture processes in ice shelves.

Acknowledgement: Calculations for this research were conducted on the Lichtenberg high performance computer of the Technische Universität Darmstadt.

REFERENCES

[1] Francfort, G. A., and Marigo, J. J. *Revisiting brittle fracture as an enerty minimization problem.* Journal of the Mechanics and Physics of Solids, 46(8), pp. 1319–1342, 1998.

[2] Bourdin, B., Francfort, G. A., and Marigo, J. J. *Numerical experiments in revisited brittle fracture.* Journal of the Mechanics and Physics of Solids, 48(4), pp. 797–826, 2000.

[3] Bourdin, B. *Numerical implementation of the variational formulation for quasi-static brittle fracture.* Interfaces and Free Boundaries, 9(3), pp. 411–430, 2007.

[4] Bourdin, B., Francfort, G. A., and Marigo, J. J. *The variational approach to fracture.* Journal of Elasticity, 91(1), pp. 5–148, 2008.

[5] Kuhn, Ch., Schlüter, A., and Müller, R. *On degradation functions in phase filed fracture models.* Comp. Mat. Sci., 108, pp. 374–384, 2015.

[6] Borden, M. J., Hughes, T. J., Landis, C. M., Anvari, A., and Lee, I. J. *A phase-field formulation for fracture in ductile materials: Finite deformation balance law derivation, plastic degradation, and stress triaxiality effects.* Computer Methods in Applied Mechanics and Egineering, 312, pp. 130–166, 2016.

[7] Sargado, J. M., Keilegavlen, E., Berre, I., and Nordbotten, J. M. *High-accuracy phase-field models for brittle fracture based on a new family of degradation functions.* Journal of the Mechanics and Physics of Solids, 111, pp. 458–489, 2018.

[8] Amor, H., Marigo, J. J., and Marini, C. *Regularized formulation of the variational brittle fracture with unilateral contact: Numerical experiments.* Journal of the Mechanics and Physics of Solids, 57, pp. 1209–1229, 2009.

[9] Miehe, C., Hofacker, M., and Welschinger, F. *A phase field model for rate-independent crack propagation: Robust algorithmic implementation based on operator splits.* Computer Methods in Applied Mechanics and Engineering, 199, pp. 2765–2778, 2010.

[10] Strobl, M. and Seelig, T. *On constitutive assumptions in phase field approaches to brittle fracture.* Procedia Structural Integrity, 2, pp. 3705–3712, 2016.

[11] Steinke, C. and Kaliske, M. *A phase-field crack model based on directional stress decomposition.* Computational Mechanics, 63, pp. 1019–1046, 2019.

[12] Karma, A., Kessler, D. A., and Levine, H. *Phase-field model of mode III dynamic fracture.* Phyiscal Review Letters, 87(4), p. 045501, 2001.

[13] Borden, M. J., Verhoosel, C. V., Scott, M. A. Hughes, T. J., and Landis, C. M. *A phase-field description of dynamic brittle failure.* Computer Methods in Applied Mechanics and Engineering, 217, pp. 77–95, 2012.

[14] Schlüter, A., Willenbücher, A., Kuhn, Ch., and Müller, R. *Phase field approximation of dynamic brittle fracture.* Comp. Mech., 54, pp. 1141–1161, 2014.

[15] Schlüter, A., Kuhn, C., Müller, R., and Gross, D. *An investigation of intersonic fracture using a phase field model.* Archive of Applied Mechanics, 86, pp. 321–333, 2016.

[16] Ren, H. L., Zhuang, X. Y., Anitescu, C., and Rabczuk, T. *An explicit phase field method for brittle dynamic fracture.* Computers & Structures, 217, pp. 45–56, 2019.

[17] Lo, Y. S., Borden, M. J., Ravi-Chandar, K., and Landis, C. M. *A phase-field model for fatigue crack growth.* Journal of the Mechanics and Physics of Solids, 132, p. 103684, 2019.

[18] Seiler, M., Linse, T., Hantschke, P., and Kästner, M. *An efficient phase-field model for fatigue fracture in ductile materials.* Egineering Fracture Mechanics, 224, p. 106807, 2020.

[19] Carrara, P., Ambati, M., Alessi, R., and De Lorenzis, L. *A framework to model the fatigue behavior of brittle materials based on a variational phase-field approach.* Computer Methods in Applied Mechanics and Engineering, 361, p. 112731, 2020.

[20] Schreiber, Ch., Kuhn, Ch., Müller, R., and Zohdi, T. *A phase field Modeling approach of cyclic fatigue crack growth.* Int. J. Fract., 225, pp. 89–100, 2020.

[21] Yan, S., Schreiber, C., and Müller, R. *An efficient implementation of a phase field model for fatigue crack growth.* International Journal of Fracture, pp. 1–14, 2022.

[22] Teichtmeister, S., Kienle, D., Aldakheel, F., and Keip, M. A. *Phase field modeling of fracture in anisotropic brittle solids.* International Journal of Non-Linear Mechanics, 97, pp. 1–21, 2017.

[23] Schreiber, C., Kuhn, C., and Müller, R. *A phase field model for materials with anisotropic fracture resistance.* In Proceedings of the 7th GACM colloquium, pp. 330–334, 2017.

[24] Bleyer, J. and Alessi, R. *Phase-field modeling of anisotropic brittle fracture including several damage mechanisms.* Computer Methods in Applied Mechanics and Engineering, 336, pp. 213–236, 2018.

[25] Gültekin, O., Dal, H., and Holzapfel, G. A. *Numerical aspects of anisotropic failure in soft biological tissues favor energy based criteria: A rate-dependent anisotropic crack phase field model.* Computer Methods in Applied Mechanics and Egineering, 331, pp. 23–52, 2018.

[26] Schreiber, C. *Phase Field Modeling of Fracture: Fatigue and Anisotropic Fracture Resistance.* Ph.D. Thesis, TU Kaiserslautern, 2021.

[27] Ambati, M., Gerasimov, T., and De Lorenzis, L. *Phase-field modeling of ductile fracture.* Computational Mechanics, 55(5), pp. 1017–1040, 2015.

[28] Miehe, C., Hofacker, M., Schänzel, L. M., and Aldakheel, F. *Phase field modeling of fracture in multi-physics problems. Part II. Coupled brittle-to-ductile failure criteria and crack propagation in thermo-elastic-plastic solids.* Computer Methods in Applied Mechanics and Engineering, 294, pp. 486–522, 2015.

[29] Miehe, C., Aldakheel, F., and Raina, A. *Phase field modeling of ductile fracture at finite strains: A variational gradient-extended plasticity-damage theory.* International Journal of Plasticity, 84, pp. 1–32, 2016.

[30] Fang, J., Wu, C., Rabczuk, T., Wu, C., Sun, G., and Li, Q. *Phase field fracture in elasto-plastic solids: Abaqus implementation and case studies.* Theoretical and Applied Fracture Mechanics, 103, p. 102252, 2019.

[31] Noll, T., Kuhn, Ch., Olesch, D., and Müller, R. *3D phase field simulations of ductile fracture.* GAMM Mitteilungen, 43, 2020.

[32] Liu, Z., Roggel, J., and Juhre, D. *Phase-field modelling of fracture in viscoelastic solids.* Proceedia Structural Integrity, 13, pp. 781–786, 2018.

[33] Shen, R., Waisman, H., and Guo, L. *Fracture of viscoelastic solids modeled with a modified phase field method.* Computer Methods in Applied Mechanics and Engineering, 346, pp. 862–890, 2019.

[34] Yin, B., and Kaliske, M. *Fracture simulation of viscoelastic polymers by the phase-field method.* Computational Mechanics, 65(2), pp. 293–309, 2020.

[35] Dammaß, F., Ambati, M., and Kästner, M., *A unified phase-field model of fracture in viscoelastic materials.* Continuum Mechanics and Thermodynamics, 1-23, 2021.

[36] Mouginot, J., Rignot, E., Scheuchl, B., Fenty, I., Khazendar, A., Morlighem, M., Buzzi, A., and Paden, J. *Fast retreat of Zachariæ Isstrøm, northeast Greenland.* Science, 350(6266), pp. 1357–1361, 2015.

[37] Joughin, I., Shean, D. E., Smith, B. E., and Floricioiu, D. *A decade of variability on Jakobshavn Isbræ: ocean temperatures pace speed through influence of mélange rigidity.* The Cryosphere, 14, pp. 211–227, 2020.

[38] Humbert, A., Gross, D., Müller, R., Braun, M., van de Wal, R., van den Broeke, M., Vaughan, D., and van de Berg, W. *Deformation and failure of the ice bridge on the Wilkins Ice Shelf, Antarctica.* Annals of Glaciology, 51, pp. 49–55, 2010.

[39] Gudmundsson, G. H. *Ice-stream response to ocean tides and the form of the basal sliding law.* The Cryosphere, 5(1), pp. 259–270, 2011.

[40] Robel, A. A., Tsai, V. C., Minchew, B., and Simons, M. *Tidal modulation of ice shelf buttressing stresses* Annals of Glaciology, 58(74), pp. 12–20, 2017.

[41] Christmann, J., Helm, V., Khan, S. A., Kleiner, T., Müller, R., Morlighem, M., Neckel, N., Rückamp, M., Steinhage, D., Zeising, O., and Humbert, A. *Elastic deformation plays a non-negligible role in Greenland's outlet glacier flow.* Communications Earth and Environment, 2(1), pp. 1–12, 2021.

[42] Haupt, P., *Continuum Mechanics and Theory of Materials.* Springer, Berlin, Heidelberg, New York, Barcelona, Hong Kong, London, Milan, Paris, Singapore, Tokyo, 2000.

[43] Christmann J., *Viscoelastic Modeling of Calving Processes at Antarctic Ice Shelves.* Ph.D. Thesis, TU Kaiserslautern, 2017.

[44] Ambrosio, L., and Tortorelli, V. M. *On the approximation of free discontinuity problems*, Boll. Un. Mat. Ital. B(7), pp. 105–123, 1992.

[45] Christmann, J., Müller, R., Webber, K. G., Isaia, D., Schader, F. H., Kipfstuhl, S., Freitag, J., and Humbert, A. *Measurement of the fracture toughness of polycrystalline bubbly ice from an Antarctic ice core.* Earth System Science Data, 7(1), pp. 87–92, 2015.

[46] Geuzaine, C., and Remacle, J.-F. *Gmsh: a three-dimensional finite element mesh generator with built-in pre- and post-processing facilities.* International Journal for Numerical Methods in Engineering 79(11), pp. 1309-1331, 2009.

[47] Alnaes, M. S., Blechta, J., Hake, J., Johansson, A., Kehlet, B., Logg, A., Richardson, C., Ring, J., Rognes, M. E. and Wells, G. N. *The FEniCS Project Version 1.5*, Archive of Numerical Software 3, 2015.

[48] Logg, A., Mardal, K.-A., Wells, G. N., et al, *Automated Solution of Differential Equations by the Finite Element Method.* Springer, 2012.

[49] Kuhn, C. and Müller, R., *A continuum phase field model for fracture.* Engineering Fracture Mechanics, 77(18), pp. 3625–3634, 2010.

[50] Kuhn, C., *Numerical and analytical investigation of a phase field model for fracture.* Ph.D. Thesis, TU Kaiserslautern, 2013.

[51] Ahrens, J., Geveci, B., Law, C. *ParaView: An End-User Tool for Large Data Visualization.* Visualization Handbook, Elsevier, 2005.

[52] Glen, J. W. *The creep of polycrystalline ice.* Proceedings of the Royal Society of London, Series A, Mathematical and Physical Sciences, 228(1175), pp. 519–538, 1955.